Fragmentation of Water by Heavy Ions

H. Luna and E. C. Montenegro

Departamento de Física, Pontifícia Universidade Católica do Rio de Janeiro, Caixa Postal 38071, Rio de Janeiro 22452-970, Brazil

(Received 22 October 2004; published 2 February 2005)

Absolute cross sections for fragmentation of water molecules by C^{3+} and O^{5+} ions over an energy region where the Bragg peak maximizes were measured for ionization, electron capture, and electron loss channels. A collision regime where $\sigma_{\Sigma_q O^{q+}} \geq \sigma_{H_2O^+}$ was reached for the first time, producing large abundances of H^+ and O^+ fragments in comparison to proton impact. Our findings have straightforward implications in the subsequent fast chemistry at the ionization site and on the O production in the first stages of water radiolysis. An unexpected channel-independent relationship between the cross sections for the fragmentation products, which is also approximately independent of the particle type, energy, and charge state, is found. A model is presented to explain such behavior allowing the cross sections of all fragmentation products to be obtained from single and double electron removal cross sections.

DOI: 10.1103/PhysRevLett.94.043201 PACS numbers: 34.50.Gb, 82.30.Fi, 87.50.–a, 95.30.–k

The fragmentation of water molecules by ionizing photons has been abundantly present in key physical, chemical, and biological phenomena since the first stages of formation of our planetary system. The products from water fragmentation follow a hierarchy which is essentially independent of the photon energy. While most of the time the ionizing radiation leaves as product the parent ion, sometimes it leaves the OH^+ radical but only as a minor product, O^+, as a signature of full water breakup [1]. These water fragments can subsequently make substantial interferences in the media where they are embedded.

Different fragmentation ratios can be obtained by different impinging particles. Although not as common as photons, there are circumstances where more powerful ionizing agents—heavy particles—appear, and water fragmentation becomes more efficient in releasing hydrogen and oxygen. The diversity of environments where ions of different kinds interact with water is broad, the water being either in the solid, vapor, or liquid phases. Some examples are (i) energetic O and S particle bombardment from the Jovian magnetosphere impinging on the icy surface of Europa produces water radiolysis which dominates the surface chemistry of that moon [2,3]; (ii) C and O ions from the solar wind interact with water molecules of cometary atmospheres leading to x-ray and UV emission phenomena [4]; (iii) ^{235}U fission fragments produce H_2 and O_2 from water fragmentation in U reactors at critical operation, with consequences on safety aspects of nuclear power plants [5], corrosion of fuel rods [6], or changing the redox state of the environment, such as in the Oklo precambrian natural fission reactor [7,8]; (iv) high energy C ions are currently being used in tumor therapy with reported good effective radiotoxic responses [9–11], taking advantage of the high ionization densities of water within the Bragg peak [12].

While photons, electrons, and protons follow the abovementioned hierarchy when inducing fragmentation of water molecules, the effects of heavy ions have remained barely known as very few measurements have been reported so far [13,14]. In the examples given above, the interaction between heavy ions and water molecules occurs within several different collision regimes and including collision channels—electron capture and electron loss—which are not present in the case of electron and photon impact. Simple inferences based on the high-velocity scaling, such as the quadratic dependence of ionization on the projectile charge, are not valid in general and the lack of information on the primary water fragmentation distributions obscures even a simple qualitative interpretation of the interacting systems as, for example, the microscopic distribution of primary radicals in C-ion treatment of tumors.

Here we report absolute cross sections for positive fragments following electron capture, ionization, and electron loss collisions of C^{3+} and O^{5+} ions on water molecules and compare the results with protons, electrons, and photons. In the proton case, absolute cross sections for water fragmentation have been measured in detail only recently [15,16]. These measurements confirmed the abovementioned concept that ionizing radiation essentially produces the ionic state of the parent molecule with decreasing fractions for the more fragmented daughters. The C-ion charge state and velocities chosen in this work correspond to those near the top of the Bragg peak where most of the energy deposit in water occurs. In this regime a substantial competition between single and multiple ionization as well as single capture and transfer-ionization channels is expected, inducing a large blowout of the water molecules at variance with the fragmentation pattern followed by photons, electrons, and protons. A broad range of dynamic possibilities for water fragmentation can thus be scanned for the first time, opening the possibility of identifying unexplored features of the fragmentation pattern.

C^{3+} and O^{5+} ions with energies from 1.0 to 3.5 MeV delivered by our 4 MV Van de Graaff accelerator collided with water vapor molecules inside an interaction chamber. An analyzing magnet placed after the collision chamber separated projectile charged products resulting from inter-

actions with the target and directed them into a position sensitive detector, placed 4 m downstream. The experimental chamber was composed of a gas cell target and a time-of-flight spectrometer. The target recoil ions were collected by a transverse electric field and passed through a high transparency grid into a field-free region before finally being detected by a second microchannel plate detector. The dissociative and nondissociative target products (H_2O^+, OH^+, O^+, O^{2+}, O^{3+}, and H^+) for electron capture, electron loss, or ionization were separated using standard coincidence techniques [17–19]. Absolute cross sections were obtained using the methodology described in Ref. [19], via the electron capture measurements. The H^+ efficiency was further verified using H_2 as a target, with the H^+ efficiencies obtained from the comparison between single and double capture, since double capture always releases a $H^+ + H^+$ pair, as well as measuring the production ratios of H^+/CH^{4+} and CH_n^+/CH_4^+ with $n = 0$–3, for 1.5 MeV proton projectiles on a CH_4 target. Our CH_4 ratios present very good agreement with those from Ref. [20].

Figure 1 shows our absolute total cross sections for the fragmentation products of H_2O and the similar cross sections for protons of Ref. [15]. While the main product with protons is H_2O^+, as expected from a sequential pathway, the main product in the C^{3+} case is H^+. The large H^+ production compared to OH^+ and O^+ in the C^{3+} case also indicates that a substantial amount of neutral OH is produced through the decay $H_2O^+ \rightarrow H^+ + OH$. Furthermore, for the whole measured energy region, it is more likely that the molecule completely explodes, releasing O^+, rather than stabilizes as OH^+.

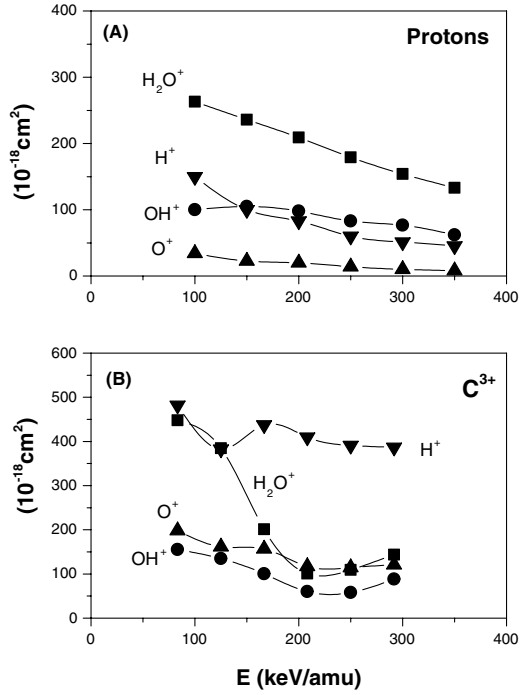

FIG. 1. Total cross sections for water fragmentation by protons [15] (a) and C^{3+} (this work) (b). The cross sections by protons follow the sequence $(H_2O^+) > (OH^+) > (O^+)$ associated with a sequential breakup process characteristic of a perturbative regime, while the C^{3+} cross sections show a very different pattern. For C^{3+}, the water is more likely to fragment completely, releasing O^+ ions, rather than to stabilize as OH^+. The experimental uncertainties for the ionization and capture channels range from $\simeq 12\%$ to 16%, while for the loss channel it is $\simeq$ 25%. Lines are drawn to guide the eyes.

The effect of the different dynamical regimes in the fragmentation of water molecules can be better viewed with the aid of Fig. 2. This ternary graph shows the normalized fractions of the H_2O^+ (P_1), OH^+ (P_2) and $\Sigma_q O^{q+}$ (P_3) cross sections for our C^{3+} and O^{5+} ionization, capture, and loss measurements, as well as data for the proton ionization of Ref. [15] in the 100–400 keV range, electron ionization from Ref. [21] in the 40–1000 eV range, 6.7 MeV/amu Xe^{44+} ionization from Ref. [13], and photofragmentation results from Ref. [1] in the 30–60 eV range. $(P_1) + (P_2) + (P_3)$ was made equal to one. Observation of the figure shows that (i) the photon, electron, and proton data are clustered around $H_2O^+ \sim 65\%$–73%, $OH^+ \sim$ 22%–30%, and $\Sigma_q O^{q+} \sim 5\%$; (ii) the heavy ions are definitively not clustered along with photons, electrons and protons; (iii) all data approximately coalesce along the straight line shown; (iv) this coalescence is, within a good approximation, independent of the nature, of the energy and of the charge state of the projectile, as well as

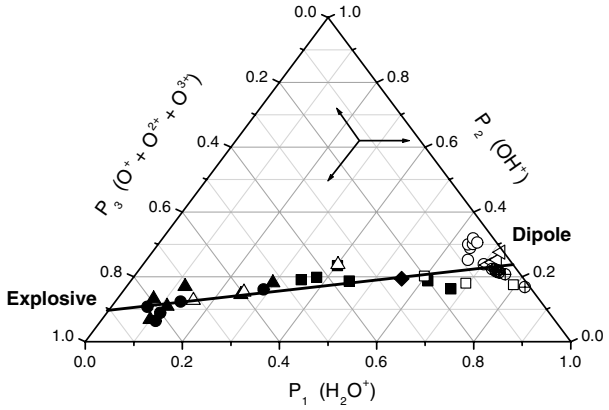

FIG. 2. Triscale plot of probabilities for H_2O^+ (P_1), OH^+ (P_2), and $\Sigma_q O^{q+}$ (P_3) formation by C^{3+} ionization (closed squares), capture (closed triangles), and loss (closed circles), O^{5+} ionization (open squares), capture (open triangles), (this work); proton ionization (open circles), (Ref. [15]); electron ionization (crossed circles) (Ref. [21]); 6.7 MeV/amu Xe^{44+} ionization (diamonds), Ref. [13]; and photofragmentation results from Ref. [1] (side open triangles). The line is a fit through the data. For the C and O data shown, the energy increases along this line from right to left for the ionization and capture channels and from left to right for the loss. Thus, electron capture and electron loss reach the explosive regime for high and low energies, respectively. The three diverging arrows in the upper side of the graph indicate how a particular data point is connected with each of the three axes.

of the collision channel which causes the fragmentation. As pointed out in Ref. [22], it is has always been assumed that the initial decomposition of water is independent of the particle type in water radiolysis modeling. Our results show that this is a good and quite general assumption for photons, electrons, and protons, but not for heavy ions. The former particles never reach the explosive regime, when the $\Sigma_q O^{q+}$ become the major fragmentation products. On the other hand, the low-velocity electron loss (circles) and high-velocity electron capture (triangles) C^{3+} data cluster around $H_2O^+ \sim 10\%$, $OH^+ \sim 10\%$, and $\Sigma_q O^{q+} \sim 80\%$. These are regimes dominated by close collisions which preferentially result in an explosive fragmentation of the water molecule.

Of particular importance for water radiolysis could be the substantial increase of O^{q+} production with C^{3+}. The O^{q+} can eventually neutralize as $O(^1D)$ or $O(^3P)$. The former reacts rapidly with water while the latter can react with OH to give HO_2 [23], supporting the suggestion that the observed increase in O_2 production by particles with high linear energy transfer (LET) is due to an increase of atomic oxygen production in primary collisions [24]. It can also be inferred from our work that the large LET of C ions is significantly consumed in blowing up water molecules, releasing O^{q+} ions and substantial amounts of energetic electrons compared with protons. This excess of energetic electrons together with the formation of high amounts of reactive water radicals would explain the different bioresponses observed with C-ion and proton tumor therapies and differences in the production of oxidizing species in water radiolysis.

To further explore the coalescence of the data we consider that the straight line shown in Fig. 2 intercepts the (P_3) axis at $(P_3) = a$ and the (P_2) axis at $(P_2) = (1 - b)$. Thus, it can be easily shown that the relation

$$P_3 = a - (a/b)(P_1) \tag{1}$$

holds. A linear fit of the measured data gives $a = 0.90$ and $b = 0.76$. From this result it follows that the *cross sections* σ_{OH^+}, $\sigma_{\Sigma_q O^{q+}}$, and $\sigma_{H_2O^+}$ are not independent but related through the equation

$$ab\sigma_{OH^+} = b(1 - a)\sigma_{\Sigma_q O^{q+}} + a(1 - b)\sigma_{H_2O^+}, \tag{2}$$

which, as shown in Fig. 2, holds, as a good approximation, for any collision channel, projectile type, and energy. This is a new result which constraints the possible H_2O dissociation pathways, independently of the collision dynamics.

The water molecule has its four valence molecular orbitals $1b_1$, $3a_1$, $1b_2$, and $2a_1$ equally populated with ionization energies of 12.6, 14.7, 18.5, and 32.2 eV, respectively [1]. Here, we assume that the cross section for one electron removal from *any one* of these states by single ionization is *the same* and that this approximation also holds for the electron capture or electron loss processes. This assumption is based on the weak dependence of the ionization [25], capture [26], and loss [27,28] cross sections on the ionization potential and on the details of the bound-state wave function in the intermediate velocity regime. We designate this cross section by σ_S^{ch}, where "ch" indicates each particular collision channel. After the electron has been removed, the water molecule either stays as a parent ion H_2O^+ with probability A_1 or fragments as OH^+ or $\Sigma_q O^{q+}$ with probabilities A_2 and A_3, respectively. Within the same reasoning, we designate as σ_D^{ch} the cross section for two-electron removal coming from either double ionization, transfer ionization, or loss-double ionization. After the removal of two electrons the water molecule fragments in OH^+ or $\Sigma_q O^{q+}$ with probabilities B_2 and B_3, respectively. We then have

$$\sigma_{H_2O^+} = A_1\sigma_S^{ch}, \tag{3}$$

$$\sigma_{OH^+} = A_2\sigma_S^{ch} + B_2\sigma_D^{ch}, \tag{4}$$

$$\sigma_{\Sigma_q O^{q+}} = A_3\sigma_S^{ch} + B_3\sigma_D^{ch}. \tag{5}$$

This system of equations establishes the constraints between the cross sections σ_{OH^+}, $\sigma_{\Sigma_q O^{q+}}$, and $\sigma_{H_2O^+}$. Indeed, it is straightforward to show that the above equa-

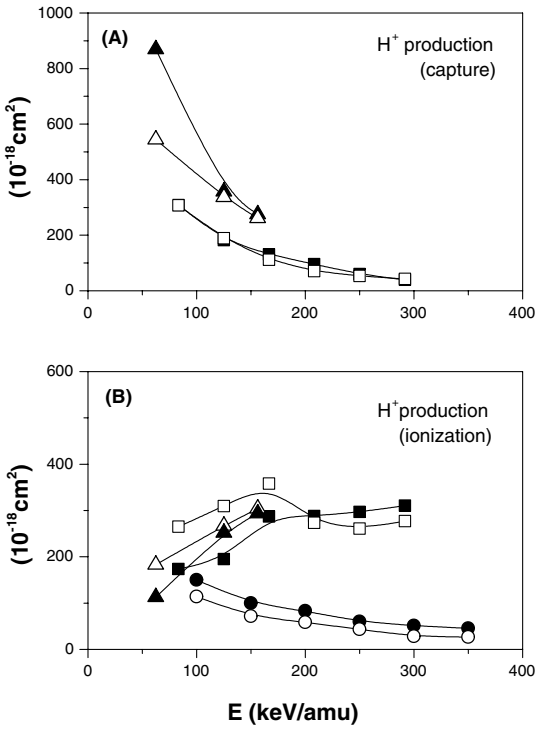

FIG. 3. H^+ production cross sections from water fragmentation induced by capture (a) and ionization (b) channels by C^{3+} (squares), O^{5+} (triangles), this work, and protons (circles), Ref. [15]. The closed symbols correspond to direct measurements, while open symbols are calculated from $\sigma_{H_2O^+}$, $\Sigma_q O^{q+}$, and σ_{OH^+} cross sections (see text). Lines are drawn to guide the eyes.

tions give $P_3 = (B_3/B_T) - [(B_3A_T/A_1B_T) - A_3/A_1]P_1$, with $A_T = A_1 + A_2 + A_3$ and $B_T = B_2 + B_3$. Comparing with Eq. (1) it immediately follows that $A_2 = [(1 - b)/b]A_1 + [(1 - a)/a]A_3$ and $B_2 = [(1 - a)/a]B_3$, as well as Eq. (2).

Then, Eqs. (3)–(5) have only three free parameters which can be adjusted by determining the H^+ production cross section from the σ_{OH^+}, $\sigma_{\Sigma_q O^{q+}}$, and $\sigma_{H_2O^+}$ cross sections. The former cross section can be written as

$$\sigma_{H^+} = (1 - A_T)\sigma_S^{ch} + (2 - B_T - B_3^{O^{2+}})\sigma_D^{ch}, \quad (6)$$

where σ_D^{ch} can be calculated as

$$\sigma_D^{ch} = [b/(1 - b)][1/(A_1B_3)][A_2\sigma_{\Sigma_q O^{q+}} - A_3\sigma_{OH^+}], \quad (7)$$

with σ_S^{ch} calculated through Eq. (3) and assuming, in writing Eq. (6), that the possible outcomes from double ionization are $OH^+ + H^+$, $O^+ + H^+$, $H^+ + H^+$ or O^{2+}. The branching ratio $B_3^{O^{2+}} = \sigma_{O^{2+}}/\sigma_D^{ch}$ is the contribution from the branch $O^{2+} + 2H$ to B_3.

Figure 3 compares the measured H^+ production cross sections associated with the ionization and capture channels, for C^{3+}, O^{5+} (this work), and protons (Ref. [15]) with the cross sections calculated using Eq. (6). The parameters $A_1 = 0.52$ and $A_3 = 0.065$ were chosen according to the decay scheme described in Ref. [1] and the parameter B_3 is found to be 0.55, 0.75, and 0.77 for the ionization, capture, and loss channels, respectively. The values of B_3 were chosen to give a best general fit using the *same* set of parameters for *all* projectiles, and $B_3^{O^{2+}}$ was found to be $\simeq B_3/3$. The good general agreement between the directly measured values of σ_{H^+} and σ_{H^+} obtained through $\sigma_{H_2O^+}$, $\sigma_{\Sigma_q O^{q+}}$, and σ_{OH^+} corroborates the consistency of our model and approximations. The key point that emerges from this analysis is the unexpected weak dependence of the coefficients A_i and B_i with the particle type, charge state, and energy, with a more visible dependence with the collision channel through the coefficients B_i, which might be an indication that the fragmentation yields are dominated by a postcollisional relaxation. This approximate universal behavior can be advantageously used to obtain fragmentation cross sections for collisions with heavy ions if, for example, reliable calculations of σ_S^{ch} and σ_D^{ch} or appropriate scaling laws are available. It should be stressed that the collisions studied in this work are outside the perturbative regime, which makes this universal behavior even more useful.

We thank M. B. Shah and G. M. Sigaud for helpful comments and suggestions. This work was supported by Brazilian agencies FAPERJ, CNPq, MCT (PRONEX), and CAPES.

[1] K. H. Tan, C. E. Brion, Ph. E. Van der Leeuw, and M. J. Van der Wiel, Chem. Phys. **29**, 299 (1978).
[2] R. W. Carlson *et al.*, Science **283**, 2062 (1999).
[3] J. F. Copper, R. E. Johnson, B. H. Mauk, H. B. Garret, and N. Gehrels, Icarus **149**, 133 (2001).
[4] T. E. Cravens, Science **296**, 1042 (2002).
[5] V. Ramshesh, Sci. Prog. **84**, 69 (2001).
[6] D. R. Olander, Y. S. Kim, W.-E. Wang, and S. K. Yagnik, J. Nucl. Mater. **270**, 11 (1999).
[7] D. J. Mossman, F. Gauthier-Lafaye, and S. E. Jackson, Precambrian Res. **106**, 135 (2001).
[8] V. Savary and M. Pagel, Geochim. Cosmochim. Acta **61**, 4479 (1997).
[9] N. Yamamoto *et al.*, Lung Cancer **42**, 87 (2003).
[10] A. Nikoghosyan *et al.*, Int. J. Radiat. Oncol. Biol. Phys. **58**, 89 (2004).
[11] D. Schulz-Ertner *et al.*, Int. J. Radiat. Oncol. Biol. Phys. **58**, 631 (2004).
[12] A. Brahme, Int. J. Radiat. Oncol. Biol. Phys. **58**, 603 (2004).
[13] G. H. Olivera, C. Caraby, P. Jardin, A. Cassimi, L. Adoui, and B. Gervais, Phys. Med. Biol. **43**, 2347 (1998).
[14] Z. D. Pesic, J.-Y. Chesnel, R. Hellhammer, B. Sulik, and N. Stolterfoht, J. Phys. B **37**, 1405 (2004).
[15] U. Werner, K. Beckord, J. Becker, and H. O. Lutz, Phys. Rev. Lett. **74**, 1962 (1995).
[16] F. Gobet, B. Farizon, M. Farizon, M. J. Gaillard, M. Carré, M. Lezius, P. Scheier, and T. D. Märk, Phys. Rev. Lett. **86**, 3751 (2001).
[17] H. Luna, E. G. Cavalcanti, J. Nickles, G. M. Sigaud, and E. C. Montenegro, J. Phys. B **36**, 4717 (2003).
[18] W. S. Melo, M. M. Sant'Anna, A. C. F. Santos, G. M. Sigaud, and E. C. Montenegro, Phys. Rev. A **60**, 1124 (1999)
[19] A. C. F. Santos, W. S. Melo, M. M. Sant'Anna, G. M. Sigaud, and E. C. Montenegro, Rev. Sci. Instrum. **73**, 2369 (2002).
[20] I. Ben-Itzhak, K. D. Carnes, D. T. Johnson, P. J. Norris, and O. L. Weaver, Phys. Rev. A **49**, 881 (1994)
[21] M. V. V. Rao, I. Iga, and S. K. Srivastava, J. Geophys. Res. **100**, 26 421 (1995).
[22] J. A. LaVerne, Radiat. Res. **153**, 487 (2000).
[23] J. Meesungnoen, A. Filali-Mouhim, N. S. Ayudhya, S. Mankhetkorn, and J. P. Jay-Gerin, Chem. Phys. Lett. **377**, 419 (2003).
[24] C. Ferradini and J. P. Jay-Gerin, Radiat. Phys. Chem. **51**, 263 (1998).
[25] E. C. Montenegro, A. C. F. Santos, and G. M. Sigaud, in *Application of Accelerators in Research and Industry*, edited by J. L. Duggan and I. L. Morgan, AIP Conf. Proc. No. 576 (AIP, New York, 2001), pp. 96–99.
[26] H. Knudsen, H. K. Haugen, and P. Hvelplund, Phys. Rev. A **23**, 597 (1981).
[27] A. B. Voitkiv, G. M. Sigaud, and E. C. Montenegro, Phys. Rev. A **59**, 2794 (1999).
[28] E. C. Montenegro, A. C. F. Santos, W. S. Melo, M. M. Sant'Anna, and G. M. Sigaud, Phys. Rev. Lett. **88**, 013201 (2002)